Supplemental information

Upregulation of antioxidant capacity and nucleotide precursor availability suffices for oncogenic transformation

Yang Zhang, Yi Xu, Wenyun Lu, Jonathan M. Ghergurovich, Lili Guo, Ian A. Blair, Joshua D. Rabinowitz, and Xiaolu Yang

Figure S1

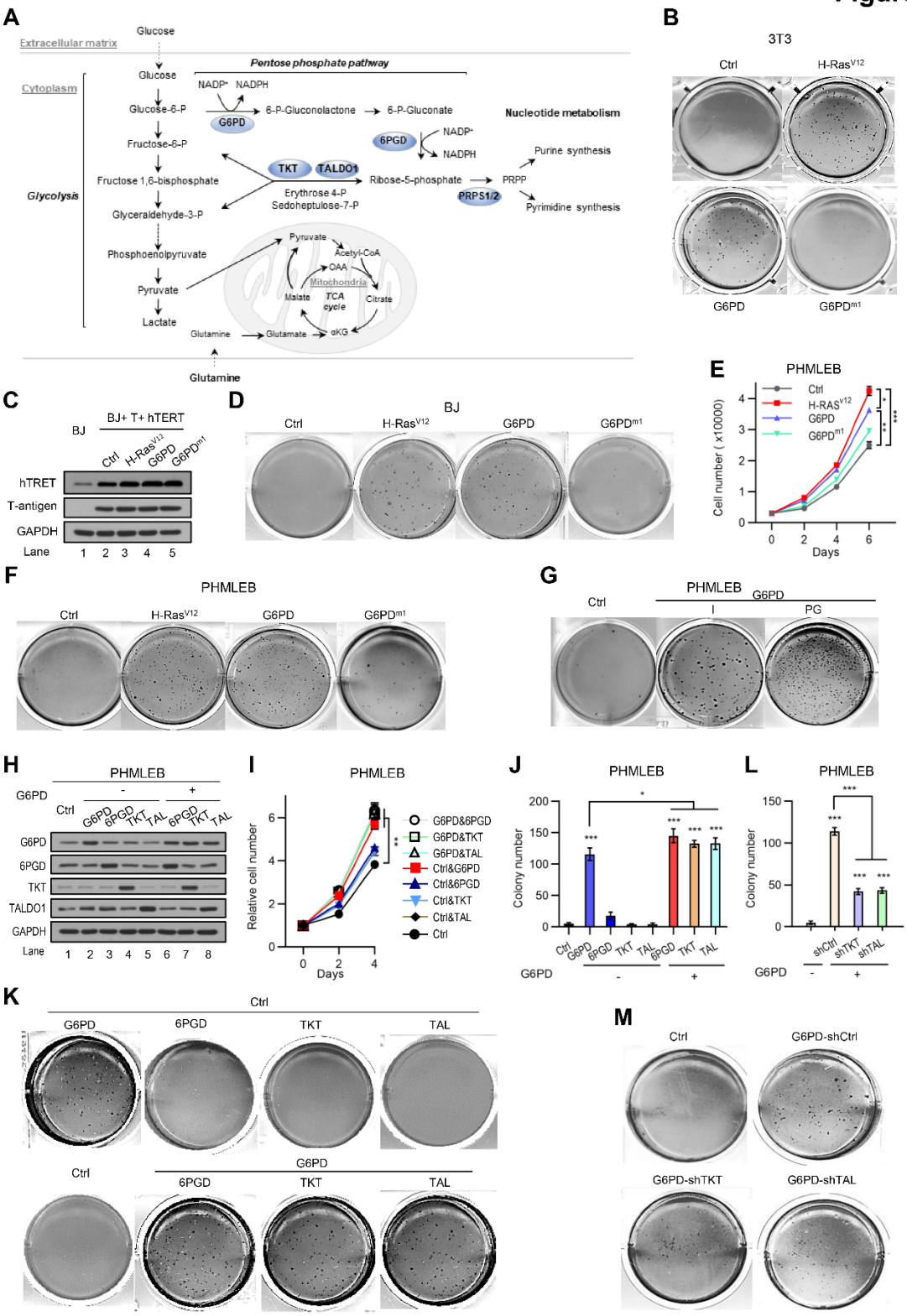
A
Extracellular matrix
Glucose
Cytoplasm
Pentose phosphate pathway
Glycolysis
Glucose-6-P
G6PD
6-P-Gluconolactone
6-P-Gluconate
6PGD
NADP+
NADPH
Nucleotide metabolism
Fructose-6-P
Fructose 1,6-bisphosphate
TKT
TALDO1
Ribose-5-phosphate
PRPP
PRPS1/2
Purine synthesis
Pyrimidine synthesis
Erythrose 4-P
Sedoheptulose-7-P
Glyceraldehyde-3-P
Phosphoenolpyruvate
Pyruvate
Lactate
Acetyl-CoA
OAA
Mitochondria
Malate
TCA cycle
Citrate
Glutamine
Glutamate
αKG
B
3T3
Ctrl
H-Ras^V12
G6PD
G6PD^m1
C
BJ
BJ+ T+ hTERT
hTRET
T-antigen
GAPDH
Lane
D
BJ
E
PHMLEB
Cell number (x10000)
Days
F
PHMLEB
G
PHMLEB
G6PD
H
PHMLEB
I
PHMLEB
Relative cell number
G6PD&6PGD
G6PD&TKT
G6PD&TAL
Ctrl&G6PD
Ctrl&6PGD
Ctrl&TKT
Ctrl&TAL
J
PHMLEB
Colony number
L
PHMLEB
shCtrl
shTKT
shTAL
K
M
G6PD-shCtrl
G6PD-shTKT
G6PD-shTAL

Figure S1. G6PD, but not other PPP enzymes, enables anchorage-independent growth of immortalized murine and human cells, related to Figure 1 and 3

(A) Schematic diagram of central glucose metabolic pathways and nucleotide synthesis.

(B) Representative images of soft agar colonies formed by NIH3T3 cells infected with retroviruses control (Ctrl) or retroviruses expressing H-Ras^{V12}, G6PD, or G6PD^{m1}. Related to Figures 1C and 1D.

(C) Protein expression in primary BJ cells, as well as BJ cells immortalized with hTERT and SV40 T-antigens (BJ+T+hTERT) infected with control, H-Ras^{V12}, G6PD, or G6PD^{m1} retroviruses.

(D and F) Representative image of soft agar colonies for BJ (D) or PHMLEB (F) cells. Related to Figures 1F and 1H.

(E) Adherent proliferation for PHMLEB cells stably transduced with control, H-Ras^{V12}, G6PD, or G6PD^{m1} retroviral vectors.

(G) Representative images of soft agar colonies formed by PHMLEB cells, as well as PHMLEB/G6PD cells previously un-grown (initial or I) or grown (PG) in soft agar. Related to Figure 1J.

(H-K) PHMLEB cells stably expressing G6PD, 6PGD, TKT, and TALDO1 (TAL) as indicated were assayed for protein expression (H), adherent proliferation (I), and soft agar colony formation with quantification of colony numbers (J) and representative images of soft agar colonies (K).

(L and M) Control (Ctrl) PHMLEB cells and PHMLEB/G6PD cells expressing control shRNA (shCrtl) or shRNA against TKT (shTKT) or TALDO1 (shTAL) were assayed for soft agar colony formation (L and M). The expression of G6PD, TKT and TALDO1 proteins is shown in Figure 3L.

Data are means ± SD of representative result (n = 3). *$P < 0.05$, **$P < 0.01$, ***$P < 0.001$.

Figure S2

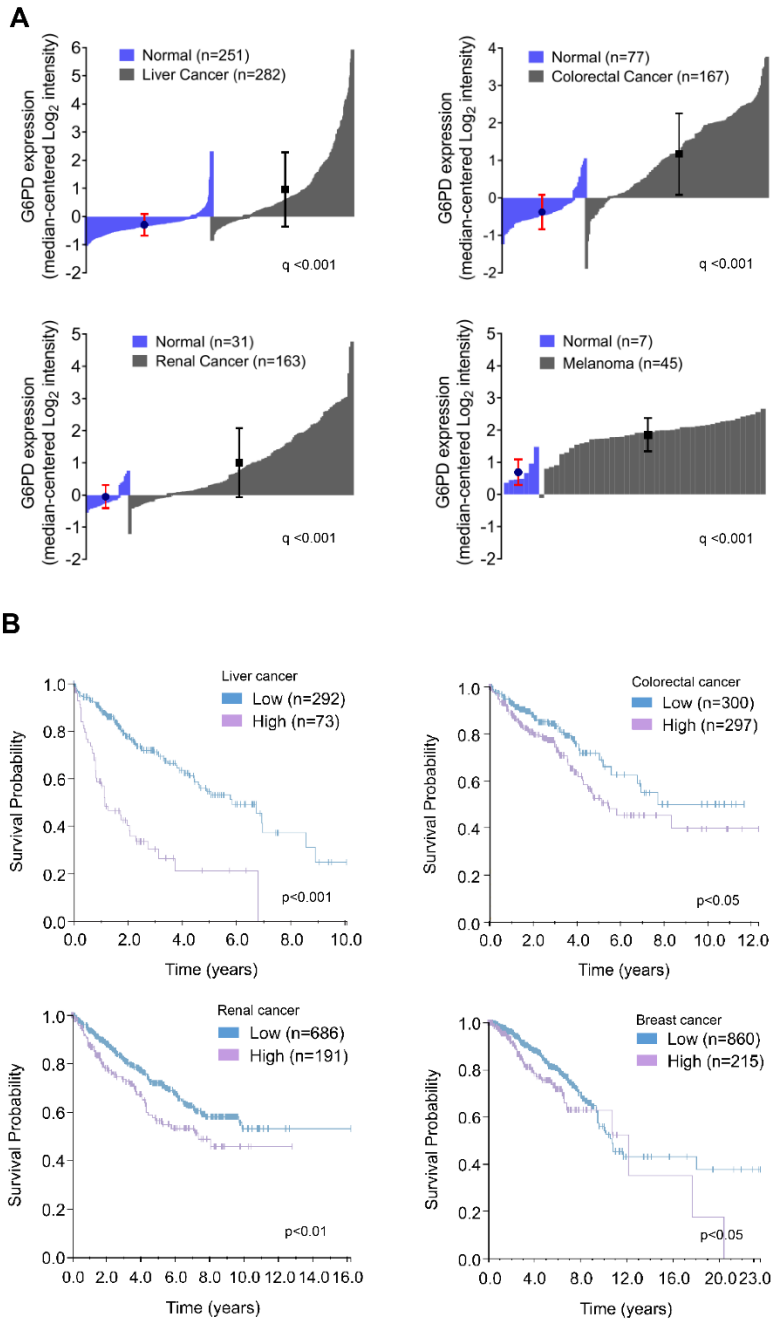

Figure S2. G6PD is upregulated in human cancers correlating with poor survival, related to Figures 1 and 2

(A) G6PD mRNA expression levels in patients of liver, colorectal, renal, and skin cancers, as well as corresponding normal controls (Oncomine database). The number of subjects included in each group and *p* value after Bonferroni correction are indicated.

(B) The survival curve of liver, colorectal, renal, and breast cancer patients with high and low G6PD expression (Human Protein Atlas database). The number of subjects included in each group and *p* value are indicated. Related to Table S1.

Figure S3

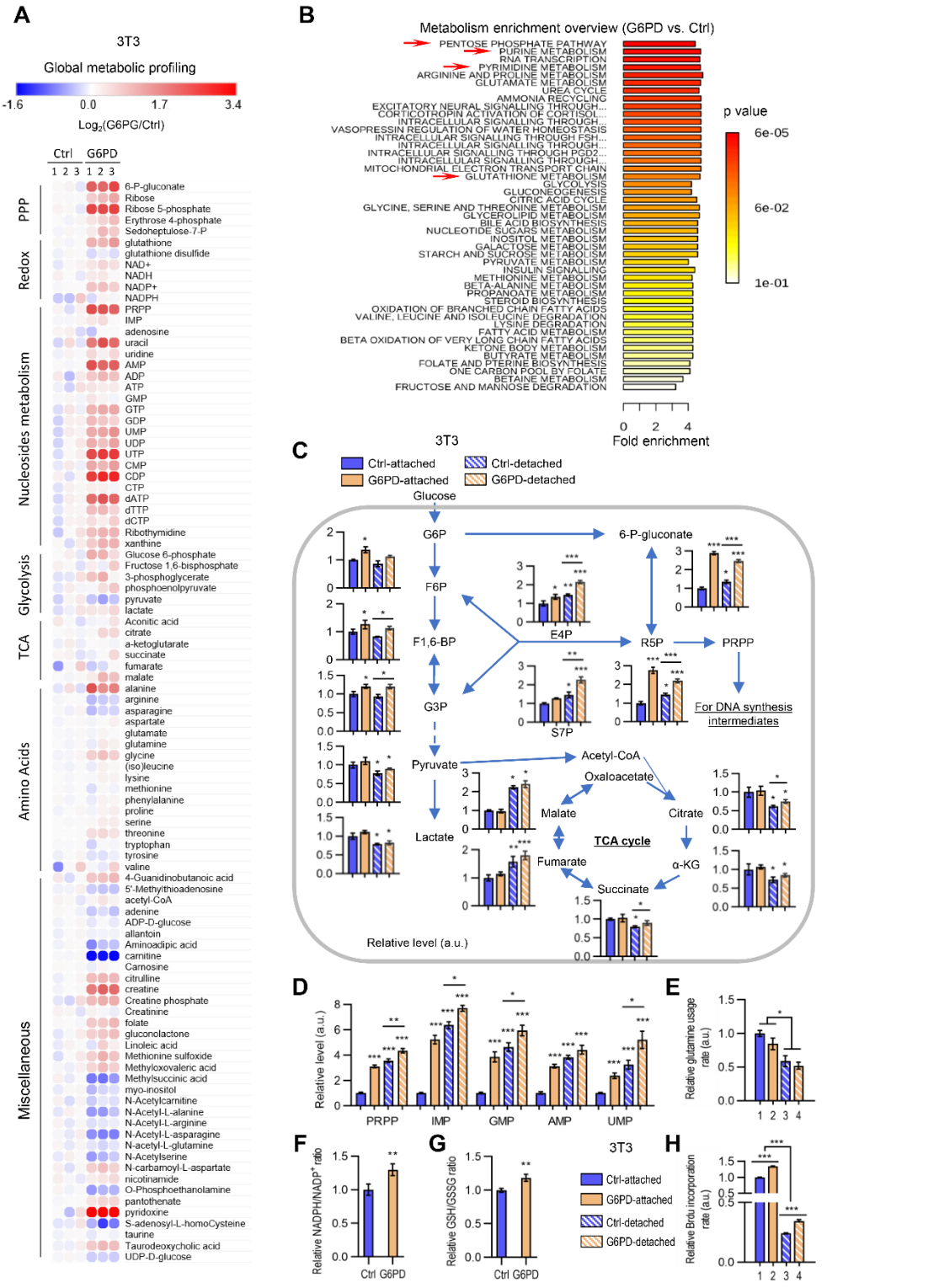
A
3T3
Global metabolic profiling
-1.6
0.0
1.7
3.4
Log2(G6PG/Ctrl)
Ctrl
G6PD
1 2 3 1 2 3
PPP
Redox
Nucleosides metabolism
Glycolysis
TCA
Amino Acids
Miscellaneous
6-P-gluconate
Ribose
Ribose 5-phosphate
Erythrose 4-phosphate
Sedoheptulose-7-P
glutathione
glutathione disulfide
NAD+
NADH
NADP+
NADPH
PRPP
IMP
adenosine
uracil
uridine
AMP
ADP
ATP
GMP
GTP
GDP
UMP
UDP
UTP
CMP
CDP
CTP
dATP
dTTP
dCTP
Ribothymidine
xanthine
Glucose 6-phosphate
Fructose 1,6-bisphosphate
3-phosphoglycerate
phosphoenolpyruvate
pyruvate
lactate
Aconitic acid
citrate
a-ketoglutarate
succinate
fumarate
malate
alanine
arginine
asparagine
aspartate
glutamate
glutamine
glycine
(iso)leucine
lysine
methionine
phenylalanine
proline
serine
threonine
tryptophan
tyrosine
valine
4-Guanidinobutanoic acid
5'-Methylthioadenosine
acetyl-CoA
adenine
ADP-D-glucose
allantoin
Aminoadipic acid
carnitine
Carnosine
citrulline
creatine
Creatine phosphate
Creatinine
folate
gluconolactone
Linoleic acid
Methionine sulfoxide
Methyloxovaleric acid
Methylsuccinic acid
myo-inositol
N-Acetylcarnitine
N-Acetyl-L-alanine
N-Acetyl-L-arginine
N-Acetyl-L-asparagine
N-acetyl-L-glutamine
N-Acetylserine
N-carbamoyl-L-aspartate
nicotinamide
O-Phosphoethanolamine
pantothenate
pyridoxine
S-adenosyl-L-homoCysteine
taurine
Taurodeoxycholic acid
UDP-D-glucose
B
Metabolism enrichment overview (G6PD vs. Ctrl)
PENTOSE PHOSPHATE PATHWAY
PURINE METABOLISM
RNA TRANSCRIPTION
PYRIMIDINE METABOLISM
ARGININE AND PROLINE METABOLISM
GLUTAMATE METABOLISM
UREA CYCLE
AMMONIA RECYCLING
EXCITATORY NEURAL SIGNALLING THROUGH...
CORTICOTROPIN ACTIVATION OF CORTISOL...
INTRACELLULAR SIGNALLING THROUGH...
VASOPRESSIN REGULATION OF WATER HOMEOSTASIS
INTRACELLULAR SIGNALLING THROUGH FSH...
INTRACELLULAR SIGNALLING THROUGH...
INTRACELLULAR SIGNALLING THROUGH PGD2...
INTRACELLULAR SIGNALLING THROUGH...
MITOCHONDRIAL ELECTRON TRANSPORT CHAIN
GLUTATHIONE METABOLISM
GLYCOLYSIS
GLUCONEOGENESIS
CITRIC ACID CYCLE
GLYCINE, SERINE AND THREONINE METABOLISM
GLYCEROLIPID METABOLISM
BILE ACID BIOSYNTHESIS
NUCLEOTIDE SUGARS METABOLISM
INOSITOL METABOLISM
GALACTOSE METABOLISM
STARCH AND SUCROSE METABOLISM
PYRUVATE METABOLISM
INSULIN SIGNALLING
METHIONINE METABOLISM
BETA-ALANINE METABOLISM
PROPANOATE METABOLISM
STEROID BIOSYNTHESIS
OXIDATION OF BRANCHED CHAIN FATTY ACIDS
VALINE, LEUCINE AND ISOLEUCINE DEGRADATION
LYSINE DEGRADATION
FATTY ACID METABOLISM
BETA OXIDATION OF VERY LONG CHAIN FATTY ACIDS
KETONE BODY METABOLISM
BUTYRATE METABOLISM
FOLATE AND PTERINE BIOSYNTHESIS
ONE CARBON POOL BY FOLATE
BETAINE METABOLISM
FRUCTOSE AND MANNOSE DEGRADATION
p value
6e-05
6e-02
1e-01
0 2 4
Fold enrichment
C
3T3
Ctrl-attached
Ctrl-detached
G6PD-attached
G6PD-detached
Glucose
G6P
6-P-gluconate
F6P
E4P
F1,6-BP
R5P
PRPP
G3P
S7P
For DNA synthesis intermediates
Pyruvate
Acetyl-CoA
Oxaloacetate
Malate
Citrate
Lactate
TCA cycle
Fumarate
α-KG
Succinate
Relative level (a.u.)
D
Relative level (a.u.)
PRPP
IMP
GMP
AMP
UMP
E
Relative glutamine usage rate (a.u.)
F
Relative NADPH/NADP+ ratio
Ctrl G6PD
G
Relative GSH/GSSG ratio
Ctrl G6PD
3T3
Ctrl-attached
G6PD-attached
Ctrl-detached
G6PD-detached
H
Relative Brdu incorporation rate (a.u.)
1 2 3 4

Figure S3. G6PD overexpression reprograms glucose metabolism under matrix-attached and -detached conditions, related to Figure 3

(A and B) Global metabolic profiles of control NIH3T3 and 3T3/G6PD cells grown on adherent plates were analyzed by LC-MS. The changes in metabolites are shown as heatmap (A) and major metabolic pathways enhanced by G6PD overexpression were identified by metabolism enrichment analysis (B).

(C-E**,** H) NIH3T3 and 3T3/G6PD cells cultured under matrix-attached or -detached conditions for 4 hr were assayed for central glucose metabolic metabolites (C) and nucleotide synthesis intermediates (D) by focused metabolic analysis, for glutamine usage (E), and for DNA synthesis by BrdU incorporation (H, normalized by cell number).

(F and G) Relative $NADPH/NADP^+$ (F) and GSH/GSSG (G) ratios in control NIH3T3 and 3T3/G6PD cells, based on the data in (A).

Data are means ± SD of representative result (n = 3). $*P < 0.05$, $**P < 0.01$, $***P < 0.001$.

Figure S4

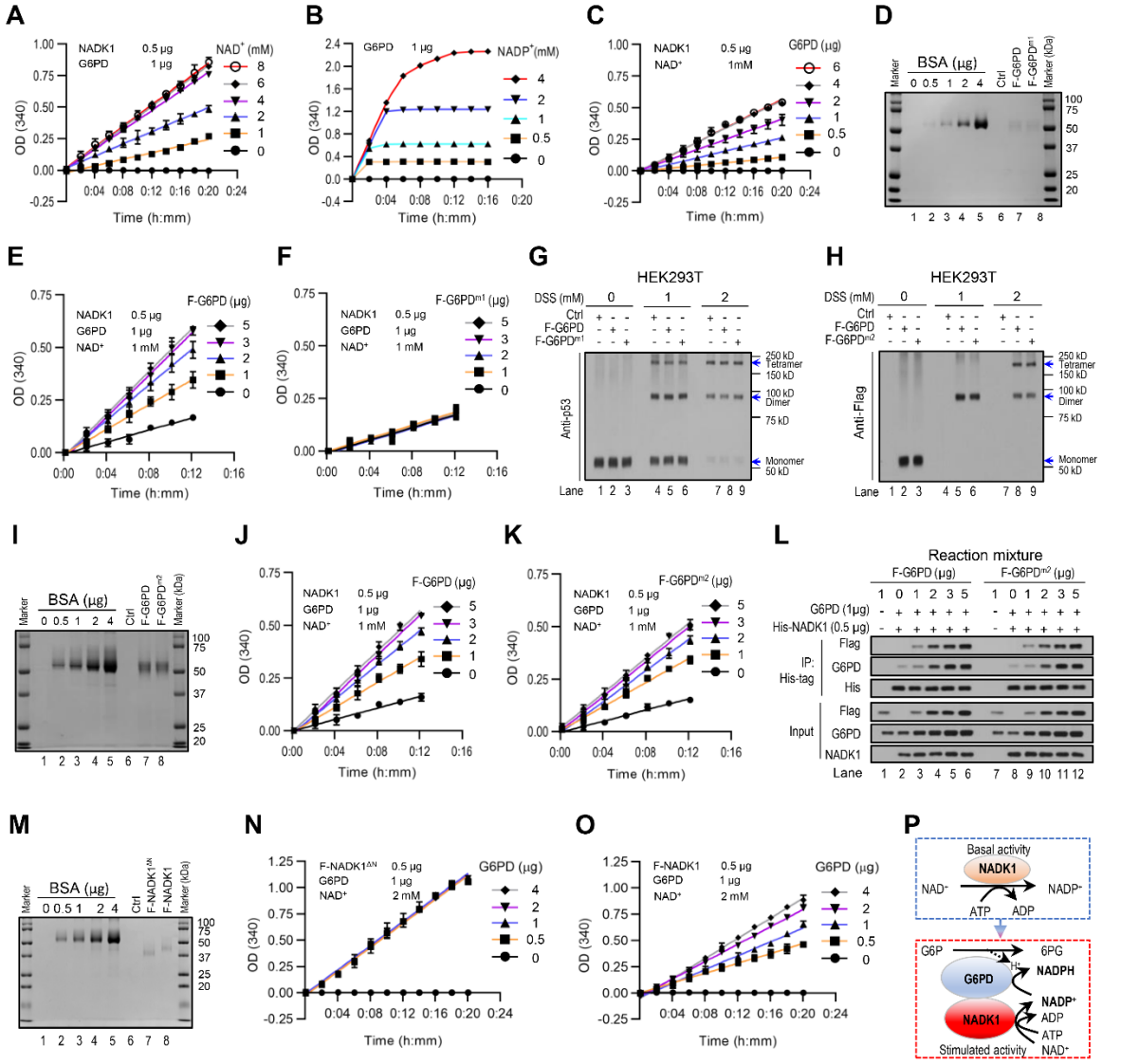

Figure S4. G6PD associates with NADK1 and counteracts its autoinhibitory N-terminal region, increasing NADK1 enzymatic activity and driving the NAD$^+$-NADP$^+$ flux, related to Figure 5

(A) NAD$^+$ at varying concentrations was converted to NADP$^+$ by 0.5 μg of 6xHis-NADK1 then to NADPH by 1 μg of G6PD purified from *E. coli* (Sigma). Generation of NADPH was monitored by OD_{340}. Related to Figure 5A.

(B) Conversion of different concentrations of NADP$^+$ to NADPH by 1 μg of G6PD was measured by OD_{340}. Note that 1 μg G6PD can convert different moles of NADP$^+$ to NADPH rapidly (B). In contrast, when the same mole of NAD$^+$ was provided and catalyzed by 0.5 μg NADK1 to NADP$^+$ and then to NADPH by 1 μg G6PD, the rates of NADPH production were dramatically reduced

(A). This indicates that NADK1-mediated $NADP^+$ production from NAD^+ is the rate-limiting step of coupled reactions.
(C) 1 mM of NAD^+ was incubated with 0.5 μg of 6xHis-NADK1 and different amounts of G6PD purified from *E coli* (Sigma). Note that at the amount of 1 μg, G6PD could convert virtually all $NADP^+$ molecules at concentrations of 2 mM or less NADPH within 4 min as shown in (B). Thus, the rate of NADPH production in the reactions containing 1 μg or more G6PD over the course of 20 min was determined by NADK1-mediated conversion of NAD^+ to $NADP^+$, rather than G6PD-mediated conversion of $NADP^+$ to NADPH. Related to Figure 5B.
(D) Coomassie blue staining of Flag-G6PD (F-G6PD) and Flag-$G6PD^{m1}$ (F-$G6PD^{m1}$) proteins purified from HEK293T cells by anti-Flag mAb beads.
(E and F) Conversion of NAD^+ to NADPH measured by OD_{340} in the presence of different amounts of Flag-G6PD (E) or Flag-$G6PD^{m1}$ (F) protein purified from HEK293T cells, 1 μg of G6PD purified from *E coli* (Sigma), 1 mM of NAD^+, and 6xHis-NADK1 (0.5 mg). Related to Figure 5C.
(G and H) HEK293T cells transfected with control, Flag-G6PD, Flag-$G6PD^{m1}$, or Flag-$G6PD^{m2}$ plasmid were treated with the indicated concentrations of DSS. Cell lysates were analyzed by Western blot for endogenous p53 (G) and Flag-tagged protein (H). p53 and G6PD/$G6PD^{m2}$ monomer, dimer, and tetramer are indicated. Endogenous p53 was used as a control for cross-linking. Note that same cross-linking conditions were used here and in Figure 5I.
(I) Coomassie blue staining of Flag-G6PD and Flag-$G6PD^{m2}$ proteins purified from HEK293T cells by anti-Flag mAb beads.
(J and K) Conversion of NAD^+ to NADPH measured by OD_{340} in the presence of different amounts of Flag-G6PD (J) or Flag-$G6PD^{m2}$ (K) protein purified from HEK293T cells, 1μg of G6PD purified from *E coli* (Sigma), 1 mM of NAD^+, and 6xHis-NADK1 (0.5 mg). Related to Figure 5N.
(L) Interaction of 6xHis-NADK1 and F-G6PD or F-$G6PD^{m2}$ in the reaction mixtures in (J) and (K) was analyzed by a pull-down assay with nickel affinity gel.
(M) Coomassie blue staining for Flag-$NADK1^{\Delta N}$ (F-$NADK1^{\Delta N}$) and Flag-NADK1 (F-NADK1) proteins purified from HEK293T cells by anti-Flag mAb beads.
(N and O) Conversion of NAD^+ to NADPH measured by OD_{340} in the presence of different amounts of G6PD protein purified from *E coli* (Sigma), 2 mM of NAD^+, and 0.5 μg of Flag-$NADK1^{\Delta N}$ (N) or Flag-NADK1 (O) protein purified from HEK293T cells. Related to Figure 5R.
(P) A model shows that the activity of NADK1 alone (top) or when associated with G6PD (bottom). G6PD may stimulate NADK1 activity through binding with N-terminal region of NADK1, counteracting its autoinhibition on the kinase domain. The G6PD-NADK1 connection links the *de novo* production of $NADP^+$ to its conversion to NADPH.
Data are means ± SD of representative result (n = 3). $*P < 0.05$, $**P < 0.01$, $***P < 0.001$.

Figure S5

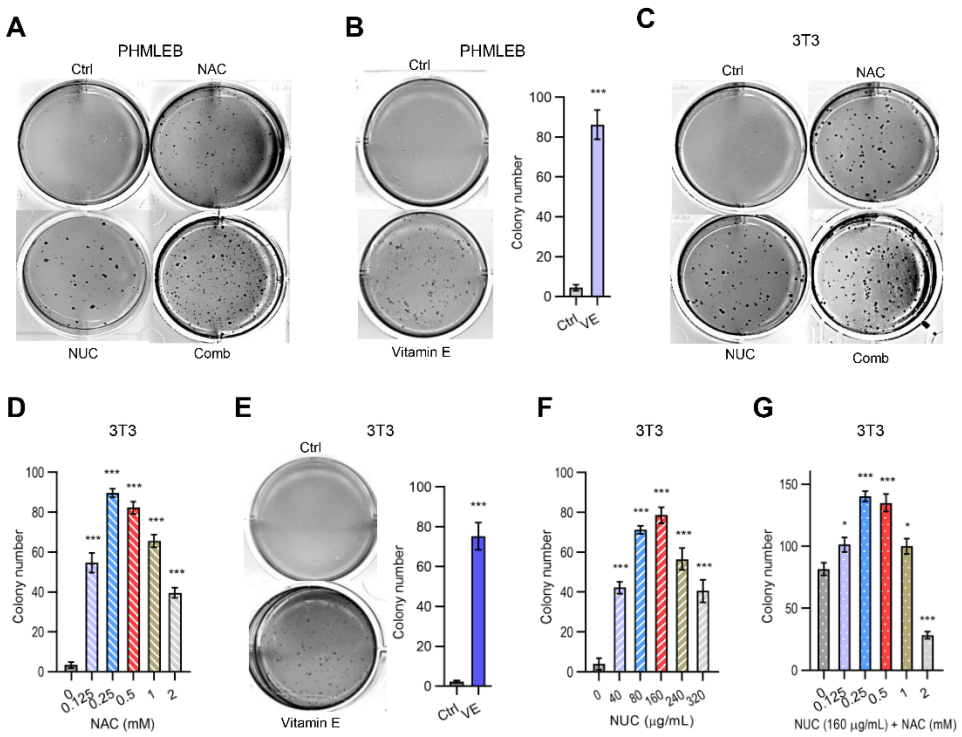

Figure S5. Antioxidants and nucleosides confer on immortalized cells anchorage-independent growth, related to Figure 6

(A, B, C, and E) Soft agar colony formation assay of PHMLEB (A and B) and NIH3T3 (C and E) cells in the presence of vehicle (Ctrl), NAC (0.25 mM), the Vitamin E (VE) derivative Trolox (0.5 mM), and/or nucleosides (NUC, 160 μg/mL) as indicated. Related to Figures 6A and 6B.

(D, F, and G) Quantification of soft agar colonies formed by NIH3T3 cells in the present different concentrations of NAC (D) or nucleosides (F), or different concentrations of NAC plus 160 μg/mL of nucleosides (G). Related to Figure 6B.

Data are means ± SD of representative result (n = 3). **P* < 0.05, ****P* < 0.001.

Figure S6

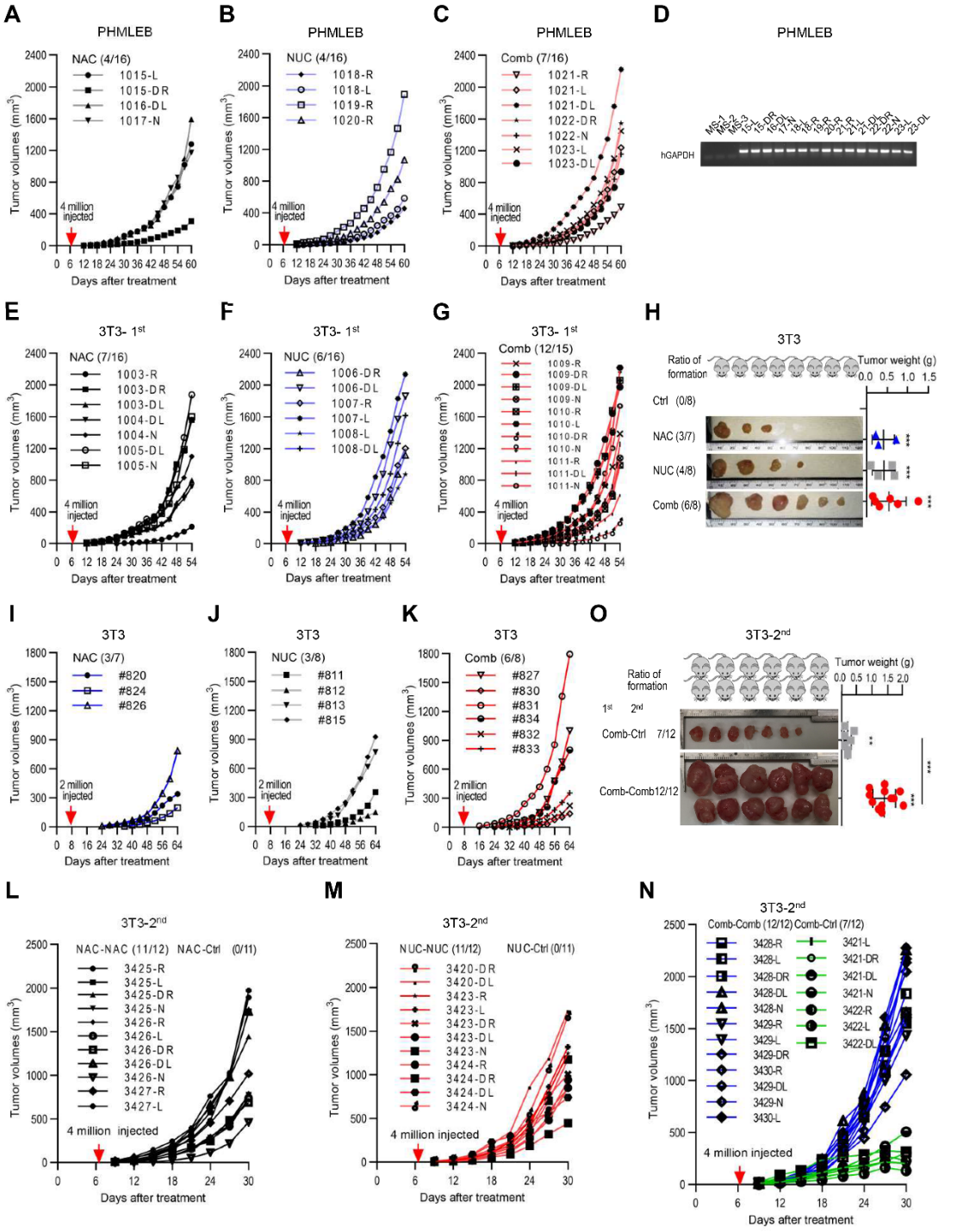

Figure S6. NAC and/or nucleosides permit tumor formation by PHMLEB cells and NIH3T3 cells in animals, and are still required for tumorigenicity when cells from initial tumors are re-inoculated in mice, related to Figure 6

(A-C) Four million of PHMLEB cells were subsequently injected into the flank of athymic nude mice supplemented with control, NAC, nucleosides (NUC), or both NAC and NUC (Comb). Shown are individual tumor growth curves (indicated as mice IDs) and the frequency of tumor formation for NAC (A), nucleosides (B), or both (C).
(D) RT-PCR analysis of human GAPDH gene (D) for tumors from (A), (B), and (C). Three mouse tissues (samples, MS1-3) were used negative controls.
(E-G and I-K) Four (E-G) or two (I-K) millions of NIH3T3 cells were injected into the flank of athymic nude mice treated with vehicle control, NAC, nucleosides, or both NAC and nucleosides (Comb) for tumor formation. Individual tumor growth curves and the frequency of tumor formation for NAC (E and I), nucleosides (F and J), or both (G and K) are shown.
(H) The frequency of tumor formation (left) and tumor images (middle) and weights (right) at the end of experiment are shown for the experiments in (I) to (K).
(L-N) Three representative tumors from each group (except control) in Figure 6D were dissected and digested with collagenase to generate single cells as described in the method. Four million of viable tumor cells were subsequently injected into the flank of new athymic nude mice for a secondary inoculation. Mice were treated with vehicle (Ctrl) or the same reagent(s) that permitted the initial tumor formation. Shown are individual tumor growth curves and the frequency of tumor formation for supplementation with NAC (L), nucleosides (M), and both NAC and nucleosides (N), as well as the corresponding controls.
(O) The frequency of tumor formation (left) and tumor images (middle) and weights (right) at the end of the experiment for (N).
Individual data and means ± SD are shown. $^{**}P < 0.01$, $^{***}P < 0.001$.

Figure S7

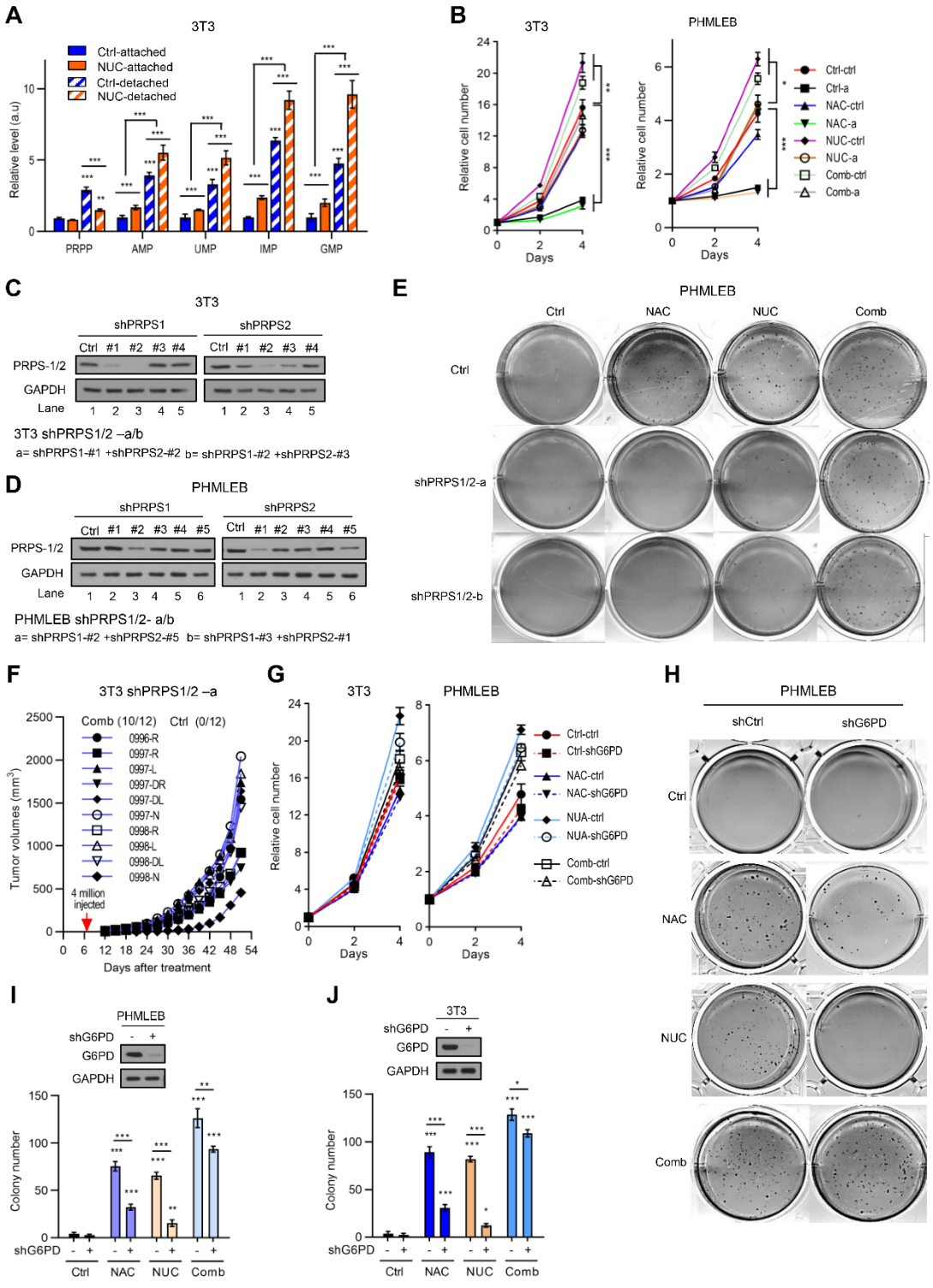
A
3T3
Ctrl-attached
NUC-attached
Ctrl-detached
NUC-detached
Relative level (a.u)
PRPP
AMP
UMP
IMP
GMP
B
3T3
PHMLEB
Relative cell number
Days
Ctrl-ctrl
Ctrl-a
NAC-ctrl
NAC-a
NUC-ctrl
NUC-a
Comb-ctrl
Comb-a
C
3T3
shPRPS1
shPRPS2
Ctrl #1 #2 #3 #4
PRPS-1/2
GAPDH
Lane
3T3 shPRPS1/2 –a/b
a= shPRPS1-#1 +shPRPS2-#2 b= shPRPS1-#2 +shPRPS2-#3
D
PHMLEB
shPRPS1
shPRPS2
Ctrl #1 #2 #3 #4 #5
PRPS-1/2
GAPDH
Lane
PHMLEB shPRPS1/2- a/b
a= shPRPS1-#2 +shPRPS2-#5 b= shPRPS1-#3 +shPRPS2-#1
E
PHMLEB
Ctrl
NAC
NUC
Comb
shPRPS1/2-a
shPRPS1/2-b
F
3T3 shPRPS1/2 –a
Comb (10/12) Ctrl (0/12)
0996-R
0997-R
0997-L
0997-DR
0997-DL
0997-N
0998-R
0998-L
0998-DL
0998-N
4 million injected
Tumor volumes (mm3)
Days after treatment
G
3T3
PHMLEB
Relative cell number
Days
Ctrl-ctrl
Ctrl-shG6PD
NAC-ctrl
NAC-shG6PD
NUA-ctrl
NUA-shG6PD
Comb-ctrl
Comb-shG6PD
H
PHMLEB
shCtrl
shG6PD
Ctrl
NAC
NUC
Comb
I
PHMLEB
shG6PD
G6PD
GAPDH
Colony number
Ctrl
NAC
NUC
Comb
J
3T3
shG6PD
G6PD
GAPDH
Colony number
Ctrl
NAC
NUC
Comb

Figure S7. Both NAC and nucleosides are required for transforming PRPS1/2- or G6PD-knockdown NIH3T3 and PHMLEB cells, related to Figure 7

(A) Intermediates of nucleotide synthesis by focused metabolic analysis for NIH3T3 cells treated with vehicle or nucleosides (160 μg/mL) and cultured for 4 hr under matrix-attached and -detached conditions.

(B) Control and PRPS1/2-knockdown (via combination "a" of PRPS1/2 shRNAs) NIH3T3 and PHMLEB cells were treated with vehicle, NAC (0.25 mM), nucleosides (160 μg/mL), or both NAC and nucleosides as indicated and assayed for adhere proliferation. The combination of PRPS1/2 shRNAs is shown in (C) and (D). The knockdown efficiency of PRPS1/2 is shown in Figures 7J and 7K.

(C and D) Screening of shRNAs for PRPS1/2 knockdown in NIH3T3 (C) and PHMLEB (D) cells. Different shRNA combinations were used to generate two populations ("a" and "b") of NIH3T3 and PHMLEB stable knockdown cells.

(E) Control and two different populations of PRPS1/2-knockdown PHMLEB cells were assayed for soft agar colony formation in the presence of vehicle (Ctrl), NAC (0.25 mM), nucleosides (160 μg/mL), or both NAC (0.25 mM) and nucleosides. Related to Figures 7K.

(F) Four million PRPS1/2-knockdown NIH3T3 cells were injected into the flank of athymic nude mice. Mice were treated with vehicle control, or NAC and nucleoside in combination, for tumor formation. Shown are the frequency of tumor formation and individual tumor growth curves for the combined treatment.

(G-J) PHMLEB (G-I) and NIH3T3 (G and J) cells with or without G6PD knockdown were treated with NAC (0.25 mM), nucleosides (160 μg/mL), or both, and assayed for adherent proliferation (G), and soft agar colony formation (H-J).

Data are means ± SD (n = 3). $*P < 0.05$, $**P < 0.01$, $***P < 0.001$.

Table S1. Statistical information of G6PD expression status and cancer patient survival, related to Figures 1, 2, and S2B

	Liver Cancer	Colorectal Cancer	Renal Cancer	Breast Cancer
Expression cut off (FPKM)	15.7	15.0	17.6	25.6
5 years survival rate- G6PD high	21%	53%	56%	75%
5 years survival rate- G6PD low	53%	69%	72%	83%
P value	9.45e-13	1.13e-2	2.89e-3	1.73e-2